

## Mechanistic Leak-Detection Modeling for Single Gas-Phase Pipelines: Lessons Learned from Fit to Field-Scale Experimental Data

A. Edrisi<sup>[a]</sup>, S. I. Kam<sup>[a],\*</sup>

<sup>[a]</sup> Craft & Hawkins Department of Petroleum Engineering, Louisiana State University, Baton Rouge, Louisiana 70803, USA.

\* Corresponding author.

Received 18 December 2012; accepted 9 March 2013

### Abstract

The use of pipelines is one of the most popular ways of delivering gas phases as shown by numerous examples in hydrocarbon transportation systems in Arctic regions, oil and gas production facilities in onshore and offshore wells, and municipal gas distribution systems in urban areas. A gas leak from pipelines can cause serious problems not only because of the financial losses associated but also its social and environmental impacts. Therefore, establishing an early leak detection model is vital to safe and secure operations of such pipeline systems.

A leak detection model for a single gas phase is presented in this study by using material balance and pressure traverse calculations. The comparison between two steady states, with and without leak, makes it possible to quantify the magnitude of disturbance in two leak detection indicators such as the change in inlet pressure ( $\Delta P_{in}$ ) and the change in outlet flow rate ( $\Delta q_{out}$ ) in a broad range of leak locations ( $x_{leak}$ ) and leak opening sizes ( $d_{leak}$ ).

The results from the fit to large-scale experimental data of Scott and Yi (1998) show that the value of leak coefficient ( $C_D$ ), which is shown to be the single-most important but largely unknown parameter, ranges from 0.55 to 4.11, and should be a function of Reynolds number ( $N_{Re}$ ) which is related to leak characteristics such as leak location ( $x_{leak}$ ), leak opening size ( $d_{leak}$ ), leak rate ( $q_{leak}$ ) and system pressure. Further investigations show that between the two leak detection indicators, the change in outlet flow rate ( $\Delta q_{out}$ ) is superior to the change in inlet pressure ( $\Delta P_{in}$ ) because of larger disturbance, if the pressure drop along the pipeline is relatively small compared to the outlet pressure; otherwise, the change in inlet pressure ( $\Delta P_{in}$ ) is superior to the change in outlet flow rate ( $\Delta q_{out}$ ).

**Key words:** Leak; Leak detection modeling; Pipeline; Leak coefficient; Gas flow in pipe

Edrisi, A., & Kam, S. I. (2013). Mechanistic Leak-Detection Modeling for Single Gas-Phase Pipelines: Lessons Learned from Fit to Field-Scale Experimental Data. *Advances in Petroleum Exploration and Development*, 5(1), 22-36. Available from: URL: <http://www.cscanada.net/index.php/aped/article/view/j.aped.1925543820130501.1027> DOI: <http://dx.doi.org/10.3968/j.aped.1925543820130501.1027>

### NOMENCLATURE

Field units are used in all equations in the text, and also all calculations are conducted based on field units.

A	cross-sectional area of leak opening
a	model parameter
b	model parameter
$C_D$	leak coefficient
$d_{leak}$	diameter of leak opening
$d_{pipe}$	inner diameter of pipeline
$f_f$	Fanning friction factor
k	specific heat capacity
L	total longitudinal length of pipeline
MF	modification factor
$N_{Re}$	Reynolds number
$P_{in}$	inlet pressure
$P_{leak}$	pressure inside the pipeline at the location of leak
$P_{out}$	outlet pressure or backpressure
$P_{up}$	pressure inside the pipeline at the location of leak
$q_{in}$	gas flowrate at the inlet
$q_{leak}$	gas flowrate leaking out through the leak
$q_{out}$	gas flowrate at the outlet
$q_{mid-}$	gas flowrate in the pipeline, infinitesimally upstream of the leak
$q_{mid+}$	gas flowrate in the pipeline, infinitesimally downstream of the leak
$T_{up}$	temperature inside the pipeline at the location of leak

- v velocity
- x longitudinal location along the pipeline
- $x_{leak}$  longitudinal location of a leak

**Greek symbols**

- $\rho$  density
- $\mu$  viscosity
- $\epsilon$  relative pipe roughness
- $\gamma_g$  gas specific gravity
- $\Delta$  difference

**Subscripts and superscripts**

- acc acceleration
- eff effective
- fri friction
- g gas
- hyd hydrostatic
- i grid block
- sc standard condition
- tot total

**INTRODUCTION**

One of the applications most sensitive to hydrocarbon leak is perhaps offshore hydrocarbon production and transportation systems as observed in the 1989 Exxon Valdez Oil Spill and the 2010 BP Oil Spill due to their devastating social, environmental and economical impacts. During recent years, increasing deepwater hydrocarbon production has been receiving a great level of attention. Relatively large field sizes and high production rates of the offshore wells are two important characteristics of deepwater oil and gas development as illustrated by the average annual oil production in Figure 1 (Minerals Management Services [MMS], 2009). However, the inevitable use of complex drilling and production facilities and long subsea pipelines poses significant challenges in terms of technology and operation (Payne, 2007; Richardson *et al.*, 2008).

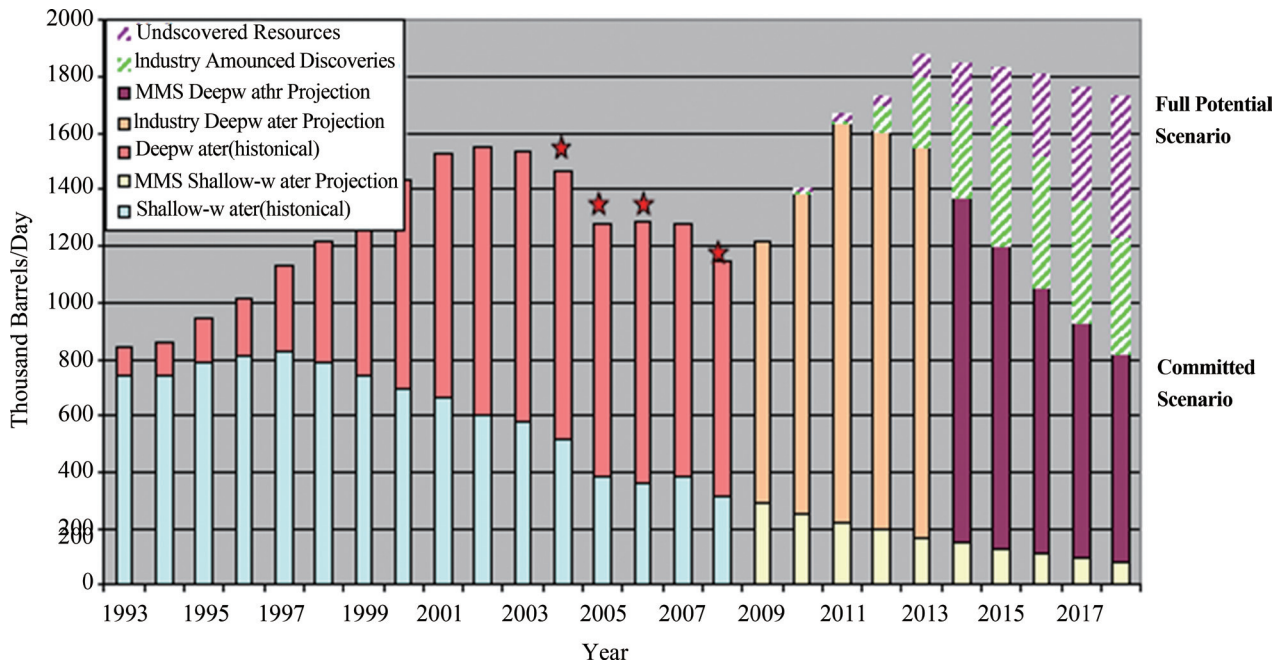


**Figure 1**  
**Gulf of Mexico Oil and Gas Production History and Forecast (MMS, 2009)**

A safe operation of natural gas and crude oil pipelines has also been an important issue in the remote geographical locations. Failure of pipeline systems has been reported in many different locations, including Alaska, China, Russia and Arctic area (Papadakis, 1999; Papadakis, Porter, & Wettig, 1999; Rosen & Schneyer, 2011; Simonoff, Restrepo, & Zimmerman, 2010; Wang & Carroll, 2007). According to U.S. department of transportation’s Pipeline and Hazardous Materials Safety Administration (PHMSA, 2010), 653 pipeline incidents were reported annually on average in the U.S. during

2005 through 2009, which resulted in an average of 456 millions of dollars per year of property damages.

Pipeline leaks are one of the major concerns in the municipal transportation and distribution systems of natural gas as well as water supply, especially when those pipelines are located near the heavily populated urban areas. A recent major incident can be found from gas explosion in San Bruno, California on September 9, 2010 when a Pacific Gas & Electric natural gas pipeline exploded in a residential area and caused not just eight people’s death, six missing and sixty injured, but millions

of dollars for repair and compensation (Berton, 2010; Hoeffel, Hennessy-Fiske, & Goffard, 2010).

Many of the leak detection approaches can be classified into two different categories: hardware-based methods using optical fiber, acoustic sensors, chemical sensors and electrical sensors; and software-based methods using fully transient computer simulations and steady-state modeling techniques (Scott & Barrufet, 2003). Because of the complexity of leak detection phenomena, it is typically believed that there is no single perfect solution—rather, a combination of different methods is highly recommended and preferred.

Recent leak detection modeling studies (Gajbhiye & Kam, 2008; Kam, 2010), which focused on the change in system response by comparing two steady states (with and without leak) in flowlines with two-phase gas-liquid mixtures, show that the steady-state modeling has good potential as part of early warning system. Those modeling studies also show that an accurate estimation of leak coefficient ( $C_D$ ), which defines how easily fluid can escape from the pipe through the leak, is critical in order to build a reliable leak detection model. Although the value of  $C_D$  is regarded as the single-most important model parameter in leak detection modeling, it has not been investigated in large field-scale leak experiments so far.

A physical phenomenon similar to pipeline leak can be found in other applications such as flow through nozzles or chokes. The suggested empirical equations typically have a proportionality constant called discharge coefficient which is similar to leak coefficient in this study (Ashford & Pierce, 1975; Gilbert, 1954; Ros, 1960; Sachdeva, Schmidt, Brill, & Blais, 1986). These studies show the magnitude of discharge coefficient depends on the design of nozzles and chokes (such as sizes and configurations), the flow of interest (such as water, oil, gas, or air), the range of flowrates passing through the system, and the surrounding conditions. For example, Ashford and Pierce (1975) show a range of 0.86-1.2 for gas-oil two-phase flow through an orifice. In both studies, the specific gravities of gas and oil were about 0.6 and 0.89 respectively, and the models were successfully compared with and verified by actual field data from an oil well. In the study of Guo, Al-Bemani, and Ghalambor (2002), the multiphase choke flow model from Sachdeva *et al.* (1986) was tested with field data from 239 gas condensate wells in Southwest Louisiana. Their recommendation was a discharge-coefficient value of 0.78, if gas phase is dominant, and 1.53, if oil phase is dominant.

By looking through the literature, similar studies for single gas-phase flow through nozzles, chokes and other constrictions can be spotted easily. Crane Company's technical book (1957) has been used as a reference in many studies, showing the following observations: (i) for nozzle-type chokes, the discharge coefficient shows a range of 0.92 - 1.2 for Reynolds Number between  $2 \times 10^3$

and  $2 \times 10^6$ ; (ii) for orifice-type chokes, a range of 0.3-1.3 for Reynolds Number of  $20-2 \times 10^6$ ; and (iii) interestingly, when Reynolds Number is above 10,000, the discharge coefficient increases with Reynolds Number for nozzle-type chokes, but decreases for orifice-type chokes. Morris (1996) shows a range of 0.67-0.95 for discharge coefficient of gas flow for most type of safety valves. Richardson, Saville, Fisher, Meredith, and Dix (2008) examined a single-phase natural gas flow through orifice with three different sizes of 8, 10 and 15 millimeter. Their results show a discharge-coefficient range of 0.86 - 0.94 for mass rates below 1 kg/s while almost constant at 0.9 for mass rates between 1-3 kg/s.

An important observation from the literature search is that many of these studies point out that the discharge coefficient is not a single fixed value, but in general is a function of flow conditions, more specifically, being linearly proportional to  $N_{Re}^{-1/2}$  (Crane Company, 1957; Guo *et al.*, 2002; Ishibashi & Takamoto, 2000; Kim, Kim, & Park, 2006).

By following the methodology presented by Gajbhiye and Kam (2008) and Kam (2010), which compares the two steady states (one with leak, and the other without leak) and presents the level of disturbance of the system as a function of leak opening size and longitudinal leak location, this study aims to extract the range of leak coefficient ( $C_D$ ) from large field-size leak detection experiments with a single gas phase, and investigates its implication in leak detection modeling. The experimental data which this modeling study is made a fit to are from Scott and Yi (1998) which carried out field-scale flow tests in the Petroleum Engineering Research & Technology Transfer Laboratory (PERTT LAB) at Louisiana State University.

Our model assumes that the two boundary conditions are fixed inlet flowrate ( $q_{in}$ ; meaning the feed-in flow rate is known at the entrance of the pipeline) and fixed outlet pressure ( $p_{out}$ ; meaning the back-pressure at the outlet of the pipeline is kept constant), and calculates the inlet pressure ( $p_{in}$ ) and the outlet flowrate ( $q_{out}$ ) in the absence and presence of leak. Therefore, the change in inlet pressure ( $\Delta p_{in}$ ) and the change in outlet flowrate ( $\Delta q_{out}$ ) serve as two leak detection indicators. It should be noted that deciding which variables should be fixed and which variables should be varied among those four parameters ( $p_{in}$ ,  $p_{out}$ ,  $q_{in}$ , and  $q_{out}$ ) for modeling purpose is somewhat arbitrary, therefore the same methodology can be applied to the cases with different boundary conditions.

## 1. METHODOLOGY

The actual flowrate of gas phase in pipelines may vary significantly along the longitudinal distance, because many of gas-phase properties such as compressibility, density, and viscosity are sensitive to pressure and temperature. We assume that the pipeline of interest can be

approximated by a one-dimensional system, represented by a number of calculation nodes, along which the properties of gas phase change as a function of pressure and temperature. The inlet of the pipeline is defined by input parameters, including pressure, temperature, and gas flow rate.

Suppose the pressure and temperature information is available at one node (let's say,  $i^{\text{th}}$  node). This allows basic gas properties to be decided, for example, gas viscosity from the correlation developed by Lee, Gonzalez, and Eakin (1966) and gas compressibility suggested by Dranchuk and Abou-Kassem (1975). Then, the total pressure gradient at that particular node,  $i$ , can be calculated by adding the contribution of three different components, i.e.,

$$\left(\frac{dP}{dx}\right)_{tot,i} = \left(\frac{dP}{dx}\right)_{hyd,i} + \left(\frac{dP}{dx}\right)_{acc,i} + \left(\frac{dP}{dx}\right)_{fri,i} \quad (1)$$

where  $dP/dx$  represents the gradient of pressure value (P) to a longitudinal location (x), and the subscripts tot, hyd, acc and fri represent total, hydrostatic, acceleration, and frictional. The term  $(dP/dx)_{fri}$  can be calculated by

$$\left(\frac{dP}{dx}\right)_{fri} = \frac{2f_f v^2}{d_{pipe}} \quad (2)$$

where Fanning friction factor,  $f_f$ , is determined by

$$f_f = \frac{16}{N_{Re}} \quad (3)$$

for laminar flow, and

$$\frac{1}{\sqrt{f_f}} = -4 \log \left\{ \frac{\epsilon}{3.7065} - \frac{5.0452}{N_{Re}} \log \left[ \frac{\epsilon^{1.1098}}{2.8257} + \left( \frac{7.149}{N_{Re}} \right) 0.8981 \right] \right\} \quad (4)$$

for turbulent flow (Chen, 1979). Note that  $N_{Re}$ ,  $\epsilon$ ,  $v$ , and  $d_{pipe}$  represent Reynolds Number, relative roughness of pipe, gas velocity, and pipe inner diameter respectively. The relative roughness ( $\epsilon$ ) of the pipe is material-dependent and is about 0.0005 for stainless steel pipeline (Moody, 1944).

Once the total pressure gradient is decided at one node ( $i^{\text{th}}$  node), then a numerical technique called "pressure traverse calculations" makes it possible to determine the pressure in the next node ( $(i+1)^{\text{th}}$  node) by using

$$P_{i+1} = P_i - \left(\frac{dP}{dx}\right)_{tot,i} \times (\Delta x)_i \quad (5)$$

where  $(\Delta x)_i$  is the longitudinal distance between  $i^{\text{th}}$  and  $(i+1)^{\text{th}}$  nodes. The change in temperature along the pipeline can be accommodated in a similar fashion if the system is under non-isothermal conditions.

Then the two leak-detection indicators, change in inlet pressure ( $\Delta P_{in}$ ) and change in outlet flow rate ( $\Delta q_{out}$ ), are defined as follows:

$$\Delta q_{out} = \frac{(q_{out} |_{no\ leak} - q_{out} |_{leak})}{q_{in} |_{no\ leak}} \times 100 \quad (6)$$

and

$$\Delta P_{in} = \frac{(p_{in} |_{no\ leak} - p_{in} |_{leak})}{p_{in} |_{no\ leak}} \times 100 \quad (7)$$

Note that both leak detection indicators are expressed in terms of percentage (%), and are greater than zero if a leak is present.

When fitting to experimental data, numerical models usually underestimate the pressure drop ( $\Delta P$ ) compared to the actual measured values due to the pipeline parts such as valves, fittings, flow constrictions, and so on. One popular way to handle this additional pressure drop is through the concept of equivalent length (Arnold & Stewart, 1998) which converts the magnitude of additional pressure drop into the equivalent pipeline length. In case of leak-detection modeling, however, it is easier to deal with this additional pressure drop by using "effective relative roughness",  $\epsilon_{eff}$ , i.e.,

$$\frac{1}{\sqrt{f_f}} = -4 \log \left\{ \frac{\epsilon_{eff}}{3.7065} - \frac{5.0452}{N_{Re}} \log \left[ \frac{\epsilon_{eff}^{1.1098}}{2.8257} + \left( \frac{7.149}{N_{Re}} \right) 0.8981 \right] \right\} \quad (8)$$

Note that Equation (8) is essentially the same as Equation (4) except that the relative roughness ( $\epsilon$ ) in Equation (4) is replaced by the effective relative roughness ( $\epsilon_{eff}$ ) in Equation (8) in order to take the additional pressure loss into account. This means that  $\epsilon_{eff} = \epsilon$ , if the additional pressure drop is negligible; otherwise,  $\epsilon_{eff} > \epsilon$ . We introduce another parameter called "modification factor", MF, to conveniently quantify the comparison between the pressure drop calculated numerically ( $\Delta P_{calculated}$ ) and the pressure drop measured experimentally ( $\Delta P_{measured}$ ), i.e.,

$$MF = \frac{\Delta P_{measured}}{\Delta P_{calculated}} \quad (9)$$

where  $MF = 1$  if the additional pressure drop is negligible; otherwise,  $MF > 1$ . The use of  $\epsilon_{eff}$  makes handling of the offset between numerical calculations and experimental data more convenient in numerical calculations, while the use of MF makes our understanding of the total pressure loss through the system simpler. Although  $\epsilon_{eff}$  and MF are proportional to each other ( $MF = 1$  corresponding to  $\epsilon_{eff} = \epsilon$ , and  $MF > 1$  corresponding to  $\epsilon_{eff} > \epsilon$ ), they are non-linearly related as shown in Equations (1) through (4).

Once occurs, a leak divides the pipeline system into three parts - exact location, and upstream and downstream of the leak, as schematically shown in Figure 2. The exact location of the leak is treated as a singularity point mathematically at which gas leaks out to the surrounding area (i.e., leaks from inside to outside of the pipeline). In other words, for a longitudinal location  $x$  ranging from the inlet ( $x=0$ ) to the outlet ( $x=L$ ), gas mass rate within  $0 \leq x < x_{leak}$  or within  $x_{leak} < x \leq L$  is uniform and unaltered, and the difference between them should be the same as gas

mass lost at the leak location (i.e.,  $x = x_{leak}$ ). These mass rates are then converted into flow rates at given pressure and temperature conditions. We use the terms  $q_{mid-}$  and  $q_{mid+}$  to represent gas flow rates within the pipeline at the infinitesimally upstream location of the leak ( $x = x_{leak-}$ ) and at the infinitesimally downstream location of the leak ( $x = x_{leak+}$ ). Then, the model calculates flow rate at the leak ( $q_{leak}$ ), which is a direct function of leak location and opening size, such that the system satisfies outlet pressure ( $P_{out}$ ) and material balance for gas mass. An iteration

process is involved to find the solution by trial-and-error methods. Once the solution is obtained, the two steady states – with and without leak – can be compared in terms of pressure profile and flow rate profile as shown in Figure 3. It should be pointed out that the loss of gas phase through a leak is represented by a discontinuity in terms of flow rate or pressure gradient vs. distance domain, and by a sharp corner in terms of pressure vs. distance domain.

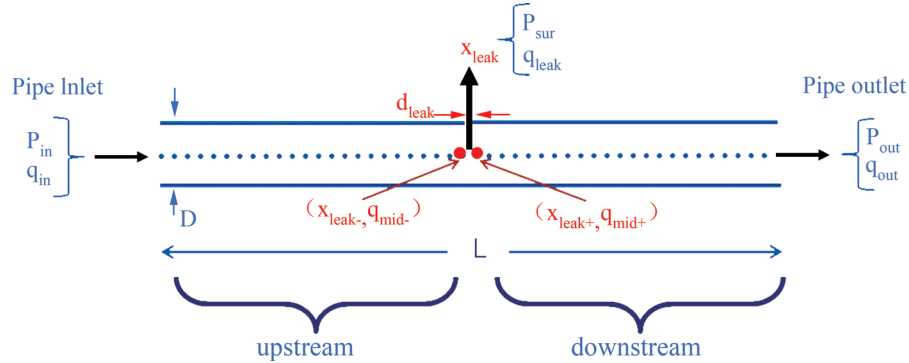


**Figure 2**  
A Schematic of the Pipeline System Investigated in this Study

The pipeline is confined by fixed inlet flowrate ( $q_{in}$ ) and outlet pressure ( $p_{out}$ ), but inlet pressure ( $p_{in}$ ) and

outlet flowrate ( $q_{out}$ ) are allowed to vary once a leak is introduced in the system.

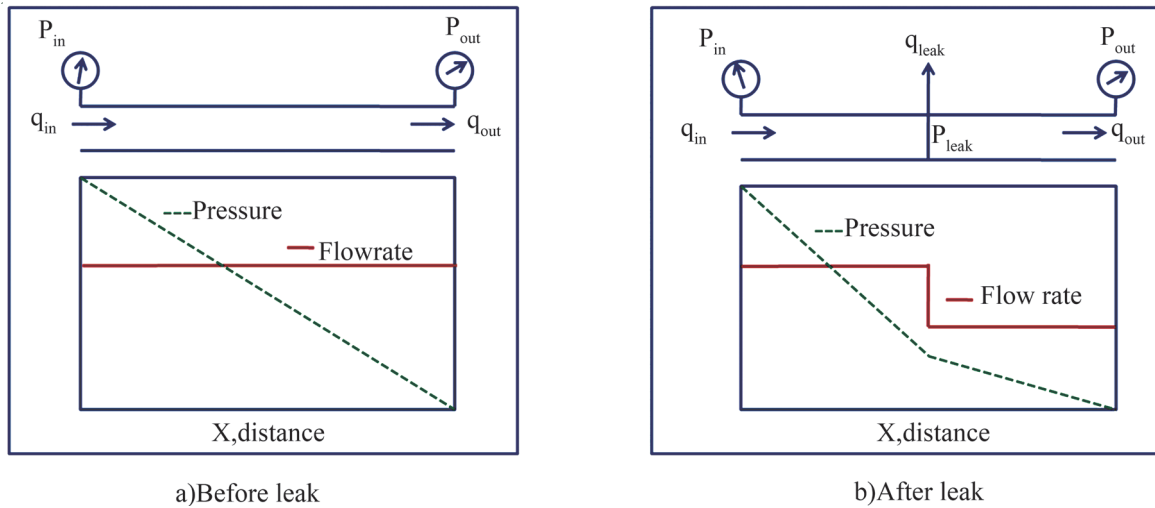


**Figure 3**  
A Schematic Showing the Comparison Between Two Steady States (Gajbhiye & Kam, 2008): a) without Leak and b) with Leak

Fluid loss at the leak location can be modeled by using equations similar to those in choke and nozzle performance (Ashford & Pierce, 1975; Gilbert, 1954; Guo, Lyons, & Ghalambor, 2007; Ros, 1960). Such equations typically relate flow rate into the pressure difference between inside and outside. This study uses an expression from Guo *et al.* (2007) which is developed for a single-phase gas sonic flow, i.e.,

$$q_{sc} = 879C_D A P_{up} \sqrt{\left(\frac{k}{\gamma_g T_{up}}\right) \left(\frac{2}{k+1}\right)^{\frac{k+1}{k-1}}} \quad (10)$$

where,  $P_{up}$  and  $T_{up}$  represent the pressure and temperature inside the pipeline at the leak location,  $q_{sc}$  and  $\gamma_g$  are gas flow rate and gas specific gravity at standard conditions,  $A$  is the leak opening size, and  $k$  is a material- and geometry-dependent constant.

Taking it into account that the focus of leak detection modeling is to predict the response of a pipeline system in relation to the amount of gas mass lost, the importance of leak coefficient,  $C_D$  in Equation (10), cannot be overemphasized. As  $C_D$  increases, the gas phase can leak out more easily (i.e., larger  $q_{sc}$  in Equation (10)) and therefore the pipeline system becomes disturbed more, which eventually leads to higher values in leak detection indicators. As pointed out earlier, the magnitude of this leak detection indicator has never been estimated from large field-scale experiments.

Some of the previous experimental studies from nozzles and chokes (Crane Company, 1957; Ishibashi & Takamoto, 2000; Kim *et al.*, 2006) show that the  $C_D$  values should be correlated to Reynolds Number ( $N_{Re}$ ) for the flow through constrictions as follows:

$$C_D = a - \frac{b}{\sqrt{N_{Re}}} \quad (11)$$

where  $a$  and  $b$  are parameters which are determined by experimental conditions including the fluid of interest and the design of apparatus. The dimensionless Reynolds Number ( $N_{Re}$ ) is defined by using fluid density ( $\rho$ ) and viscosity ( $\mu$ ), velocity ( $v$ ), and conduit or opening diameter ( $d$ ) in the following way:

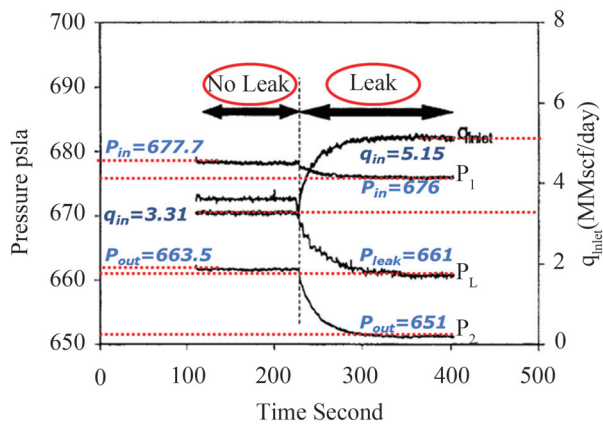


**Figure 4**  
**Reading Pressures and Flowrates from the Original Data of Scott and Yi (1998): Our Reading is Shown in Italic**

Figure 5 shows the profiles of pressure and flow rate as a function of distance when there is no leak in the pipeline. Notice that the inlet and outlet pressure values ( $P_{in}$  and  $P_{out}$ ) read in Figure 4 are shown by the “X” marks. The dashed line represents the pressure profile without introducing the effective relative roughness ( $\epsilon_{eff}$  in Equation (8)) or the modification factor (MF in Equation (9)). As a result, when the inlet injection conditions in terms of  $P_{in}$  and  $q_{in}$  are specified, the calculated outlet pressure ( $P_{out}$ ; shown by the filled “O” mark in Figure 5) is higher than the measured outlet pressure. Our model iterates the calculations by using different values of  $\epsilon_{eff}$

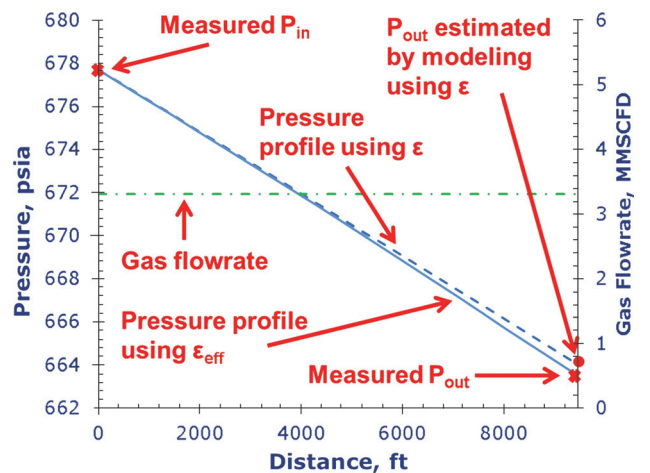
$$N_{Re} = \frac{pvd}{\mu} \quad (12)$$

## 2. RESULTS AND DISCUSSIONS

The large-scale experiments to which our model intends to fit have the following test conditions: methane as a gas phase; 9,460 ft (about 1.8 miles) long horizontal flow loops; 3.64 and 4.5 inch inner and outer diameter pipes; outlet pressure around 610 to 680 psia; injection gas flow rates around 1 to 6 MMscf/day; leak location in the middle of the pipeline; and three leak opening sizes with the diameters of 1/8, 1/4, and 3/8 inches. See Scott and Yi (1998) for more detailed information.

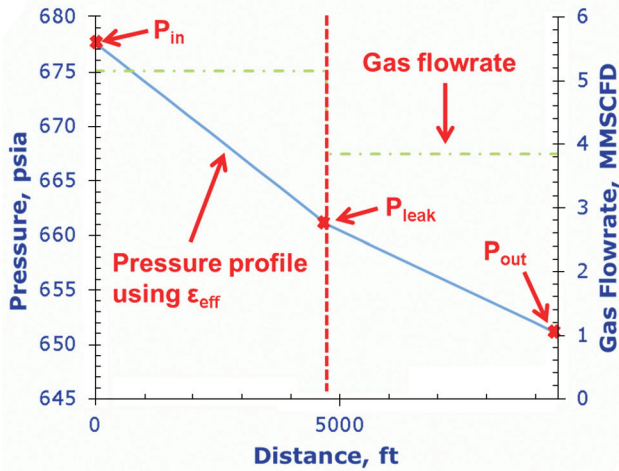
### 2.1 Response without Leak vs. Response with Leak

Figure 4 shows an example demonstrating how the system response shifts from one steady state (i.e., without leak) to another steady state (i.e., with leak) from Scott and Yi (1998). The readings for our modeling purpose are written in italic and shown as follows: (i)  $P_{in} = 677.7$  psia,  $P_{out} = 663.5$  psia, and  $q_{in} = 3.31$  MMscf/day for the system with no leak; and (ii)  $P_{in} = 676$  psia,  $P_{out} = 651$  psia,  $P_{leak} = 661$  psia, and  $q_{in} = 5.15$  MMscf/day for the system with leak.



**Figure 5**  
**Steady-State Pressure and Flowrate Profiles from the Model Fit to No-Leak Experimental Data from Figure 4**

and finds a reasonable match within the error allowance automatically. Note that the determination of  $\epsilon_{eff}$  shown in Equation (8) is affected by  $N_{Re}$ , and thus  $\epsilon_{eff}$  values are different in all nodes due to gas compressibility. In this particular case shown in Figure 5, the modification factor (MF) is 1.04. The corrected pressure profile (i.e., pressure profile with  $\epsilon_{eff}$ ) shown by the solid line in Figure 5 now is consistent with the inlet and outlet pressure values shown by “X” marks. For the rest of modeling in this study, the same procedures using  $\epsilon_{eff}$  and MF are taken to calibrate our model to the measured pressure data ( $P_{in}$  and  $P_{out}$ ) in the absence of leak.



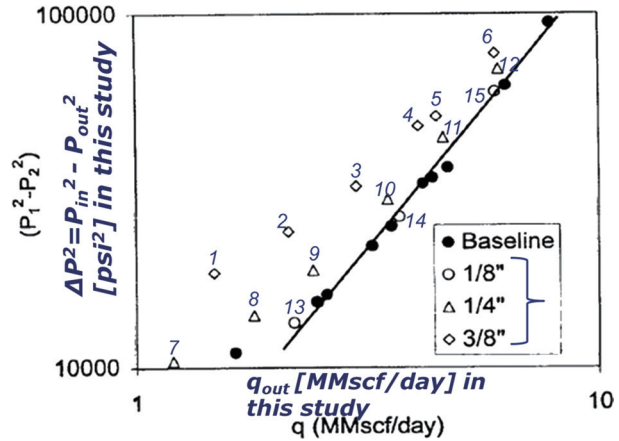
**Figure 6**  
Steady-State Pressure and Flowrate Profiles from the Model Fit to Leak Experimental Data from Figure 4

Figure 6 shows the profiles of pressure and flow rate which compare with data in Figure 4 in presence of leak. With the inlet pressure ( $P_{in}$ ) specified as part of boundary condition, the pressure profile in presence of leak is shown to be in good agreement with the outlet pressure ( $P_{out}$ ). Note that the pressure profile is calculated by using the  $\epsilon_{eff}$  values determined by Figure 5. One may notice from Figure 4 that, in typical real-world large-scale experiments, the boundary conditions that we specified for modeling purpose (i.e., fixed inlet pressure ( $P_{in}$ ) and outlet flow rate ( $q_{out}$ ) in this study) are not always kept well necessarily, and as a result the pressures and flow rates in both inlet and outlet may shift significantly. In such a case, another set of no-leak pressure and flow rate profiles should be constructed similar to Figure 5, as if these new  $P_{in}$  and  $q_{out}$  were not altered between no-leak and leak cases.

**Table 1**  
Summary of Model Fit to Large-Scale Experiments from Scott and Yi (1998)

Data No.	$d_{leak}$ , in	$\Delta P^2$	$P_{in}$ , psia	$P_{out}$ , psia	$q_{out}$ , MMscf/d	$P_{leak}$ , psia	$q_{mid}$ , MMscf/d	$q_{mid}$ , MMscf/d	$\Delta P$ , psia	$q_{leak}$ , MMscf/d	$C_D$
1	3/8	19048	676	661.76	1.56	663.40	4.48	1.56	14.24	2.92	1.16
2	3/8	25000	676	657.25	2.17	660.43	4.98	2.17	18.75	2.81	1.12
3	3/8	36745	676	648.25	3	654.36	5.86	3	27.75	2.86	1.16
4	3/8	48571	676	639.07	4.09	650.53	6.36	4.09	36.93	2.27	0.92
5	3/8	51818	676	636.52	4.5	650.39	6.37	4.5	39.48	1.87	0.76
6	3/8	77500	676	616.02	6	641.20	7.41	6	59.98	1.41	0.58
7	1/4	10476	676	668.21	1.26	669.28	3.26	1.26	7.79	2.00	1.78
8	1/4	15000	676	664.81	1.85	667.11	3.76	1.85	11.19	1.91	1.70
9	1/4	19286	676	661.58	2.47	665.68	4.05	2.47	14.42	1.58	1.41
10	1/4	30000	676	653.43	3.55	661.92	4.73	3.55	22.57	1.18	1.06
11	1/4	45000	676	641.85	4.62	656.36	5.59	4.62	34.15	0.97	0.88
12	1/4	70000	676	622.07	6.09	647.76	6.69	6.09	53.93	0.60	0.55
13	1/8	14286	676	665.35	2.24	668.72	3.40	2.24	10.65	1.16	4.11
14	1/8	27347	676	655.46	3.74	664.84	4.21	3.74	20.54	0.47	1.69
15	1/8	60526	676	629.64	5.96	653.99	5.91	5.96	46.36	-0.05	-0.17

Our analysis from the modeling study in presence of leak is shown in Table 1. As shown in Figure 7, there are a total of 15 data points (three, six, and six data points for  $d_{leak} = 1/8, 1/4$  and  $3/8$  inches respectively) showing the



**Figure 7**  
Reading 15 Data Points from the Original Experimental Data of Scott and Yi (1998) at Three Different Leak Opening Sizes of 1/8, 1/4 and 3/8 Inches in Order to Calculate  $C_D$  Values: Numbers Written in Italic are Our Reading Consistent with Those in Table 1

The procedures explained in Figures 4 through 6 can be applied to analyze the large amount of data in Figure 7, where the change in pressure response expressed on the y axis is plotted as a function of gas flow rate on the x axis at three different leak opening diameters ( $d_{leak}$ ) of 1/8, 1/4 and 3/8 inches. This original plot from Scott and Yi (1998) has the y axis equivalent to  $\Delta P^2$  (or,  $P_{in}^2 - P_{out}^2$ ) and the x axis equivalent to  $q_{out}$ , if the notations used in this study are followed. For simplicity and better comparison, the inlet pressure is assumed to be fixed at 676 psia in all these 15 experiments although it slightly varies one experiment to the other.

steady-state conditions in presence of leak. Note that the steady state with no leak is set to be  $P_{in} = 676$  psia,  $P_{out} = 643.37$  psia,  $\Delta P = P_{out} - P_{in} = 32.63$  psi and  $q_{in} = q_{out} = 5$  MMscf/day consistently for all data points as a basis

for calculations. We believe that this does not impact our calculation results noticeably because the condition at no-leak steady state only varies slightly from one experiment to another. The pressure response ( $\Delta P^2 = P_{in}^2 - P_{out}^2$ ) in the 3<sup>rd</sup> column allows us to determine  $P_{out}$  in the 5<sup>th</sup> column, while the outlet flow rate ( $q_{out}$ ) in the 6<sup>th</sup> column allows us to calculate the pressure at the leak ( $P_{leak}$ ) in the 7<sup>th</sup> column. The flow rates infinitesimally upstream or downstream locations of the leak ( $q_{mid-}$  and  $q_{mid+}$ ) are shown in the 8<sup>th</sup> and 9<sup>th</sup> columns (cf. Figure 2), and the difference between them (i.e.,  $q_{mid-} - q_{mid+}$ ) is no other than  $q_{leak}$  in the 11<sup>th</sup> column. All this information can be used to determine the values of leak coefficient ( $C_D$ ) as shown in the last 12<sup>th</sup> column. Note that for each of these 15 experiments, numerical calculations should be carried out to plot the steady-state pressure and flow rate profiles as shown in Figures 5 and 6.

This modeling result in Table 1 provides us a good insight into large-scale leak-detection problems: (i) regarding the general range of leak coefficient ( $C_D$ ), the result suggests that the typical value of  $C_D$  varies between 0.55 and 4.11, if one experiment which ends up with a negative  $C_D$  value (i.e., Data No. 15 in Table 1) is not taken into consideration; and (ii) at a given leak opening size,  $C_D$  tends to increase systematically with decreasing  $q_{out}$  or increasing  $P_{out}$ , which therefore increases with increasing  $q_{leak}$ . This means that  $C_D$  is not a constant (cf. Equation (10)) and thus should be regarded as a function of flow rate at the leak ( $q_{leak}$ ). These aspects are believed to be very important for the analysis of field-scale leak-

detection problem. It is not clear at this stage, however, why the range of  $C_D$  for  $d_{leak} = 1/8$  inch is wider compared to that for  $d_{leak} = 1/4$  or  $3/8$  inch. One possible explanation is that large-scale experiments with a smaller leak opening size take more time to reach a steady state, and it is more difficult to read pressure and flow rate values accurately due to relatively smaller system disturbance. In other words, if the noise level associated with field-scale experiments is relatively high, the accurate measurements for a smaller leak size can be more difficult.

## 2.2 Construction of Contour Maps for Leak Detection Indicators

Our next step is to investigate the effect of leak in the system in terms of the two leak detection indicators (i.e., inlet pressure ( $P_{in}$ ) and outlet flow rate ( $q_{out}$ )) at different leak locations and opening sizes. It should be mentioned that the summary in Table 1 allows us to estimate the magnitude of  $C_D$  values to be applied to the large-scale leak detection problems. More specifically, we examine four different scenarios: Case 1, the smallest  $C_D$  value ( $C_D = 0.55$ ) extracted from experimental data; Case 2, the largest  $C_D$  value ( $C_D = 4.11$ ); Case 3, the second largest  $C_D$  value ( $C_D = 1.78$ ); and Case 4,  $C_D$  value as a function of Reynolds Number as shown in Equation (10) which is related to leak characteristics such as leak rate ( $q_{leak}$ ), leak location ( $x_{leak}$ ) and leak opening size ( $d_{leak}$ ). The results of our numerical calculations are presented by using contours with  $\Delta P_{in}$  or  $\Delta q_{out}$  (as shown in Eqs. (6) and (7)) as a function of  $x_{leak}$  and  $d_{leak}$ , similar to the previous studies (Gajbhiye & Kam, 2008; Kam, 2010).

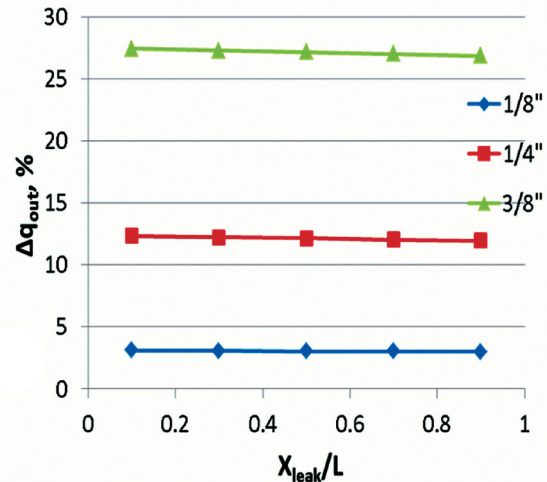
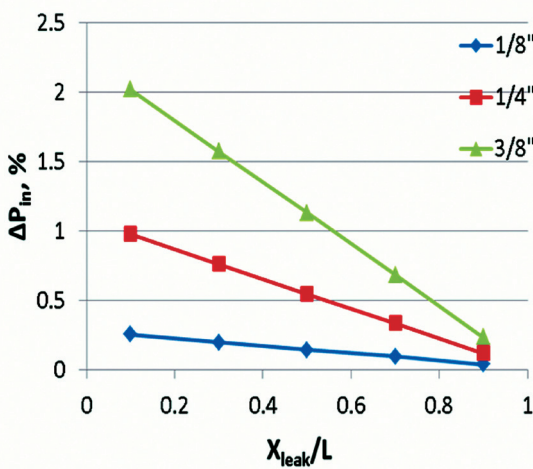


**Figure 8**  
**Changes in Leak Detection Indicators at Different Leak Opening Sizes ( $d_{leak}/d_{pipe}$ ) and Different Longitudinal Leak Locations ( $x_{leak}/L$ ) for Case 1 with  $C_D = 0.55$**

Figure 8 shows the outcomes of model runs for Case 1 with  $C_D = 0.55$ . We first fix the longitudinal location of the leak ( $x_{leak}/L$ ) and investigate the changes in leak detection indicators at different leak opening sizes ( $d_{leak}/d_{pipe}$ ). A repetition of model calculations at different leak locations makes it possible to draw the change in inlet pressure ( $\Delta P_{in}$ ) and the change in outlet flowrate ( $\Delta q_{out}$ ) as shown

in Figures 8(a) and 8(b). Note that the leak locations and leak opening sizes are expressed dimensionless – for example,  $x_{leak}/L = 0.25$  represents a leak positioned at the one quarter of the pipeline length from the inlet, and  $d_{leak}/d_{pipe} = 0.05$  represents that the leak opening diameter is about 5% of the pipe diameter. Note that the three leak opening sizes ( $d_{leak}$ ) of 1/8, 1/4, 3/8 inches correspond to

the dimensionless leak opening size ( $d_{leak}/d_{pipe}$ ) of 0.0343, 0.0687, and 0.1030. The results show that both  $\Delta P_{in}$  and  $\Delta q_{out}$  increase as leak opening size increases at a given leak location, or as leak location approaches near the inlet at a given leak opening size. This is because mass balance

plays a major role in this leak detection modeling (cf. Figure 2) – the more gas leaks out of the pipeline (due to larger opening size or due to higher pressure at the leak upstream), the more disturbance leak detection indicators exhibit.

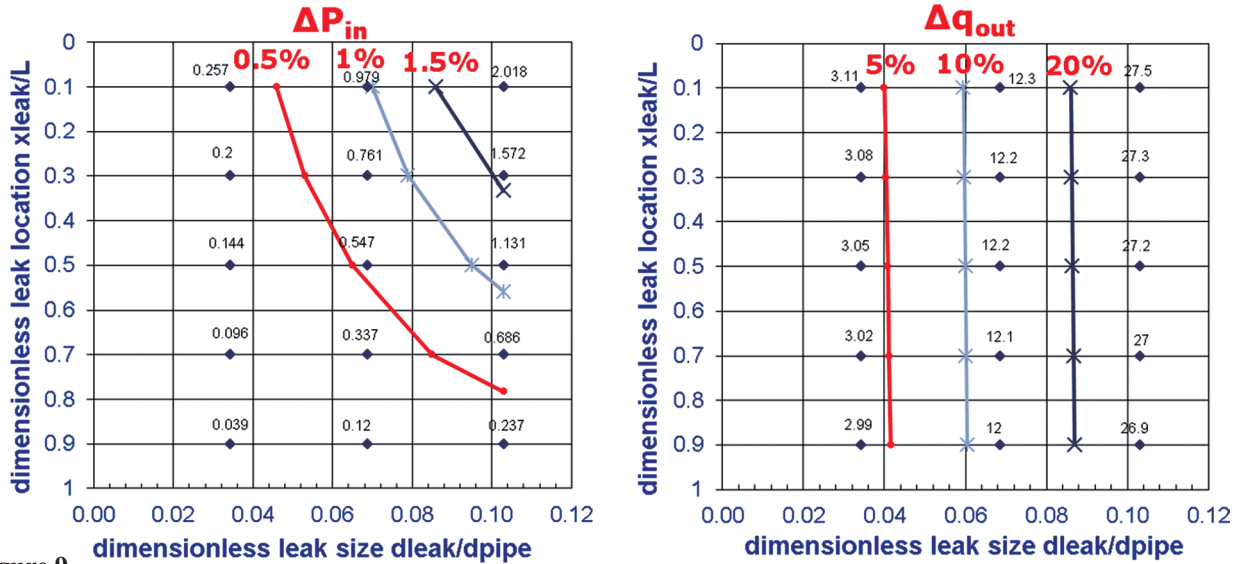


Figure 9 Contour Plots Showing the Changes in Leak Detection Indicators with and without Leak for the Smallest  $C_D$  ( $C_D=0.554$ ): (a) Change in Inlet Pressure ( $\Delta P_{in}$ ), (b) Change in Outlet Flowrate ( $\Delta q_{out}$ )

Figures 9(a) and 9(b) show the same numerical calculation results in a format of contours for  $\Delta P_{in}$  and  $\Delta q_{out}$ . The individual data points represent the leak opening size and location of interest, and values written next to them represent calculated magnitudes of disturbance in term of  $\Delta P_{in}$  and  $\Delta q_{out}$ . The y axis is constructed such that the dimensionless leak location at the outlet (i.e.,  $x_{leak}/L = 1$ ) is intersecting the x axis at the dimensionless leak size of zero (i.e.,  $d_{leak}/d_{pipe} = 0.0$ ). The contour lines are constructed by conducting linear interpolation between

two adjacent data points. The result plotted in this way provides a means of analyzing the overall impact of a leak conveniently. For example, for a leak positioned in the middle of pipeline ( $x_{leak}/L = 0.5$ ) with the opening size of 3/8 inches diameter ( $d_{leak}/d_{pipe} = 0.1030$ ), the expected level of disturbance between the two steady states (without leak vs. with leak) is approximately 1.131 % in term of  $\Delta P_{in}$  and 27.2 % in terms of  $\Delta q_{out}$ . This implies that the presence of this particular leak cannot be identified with  $\Delta P_{in}$  if the noise level is equal to or greater than 1.131 %.

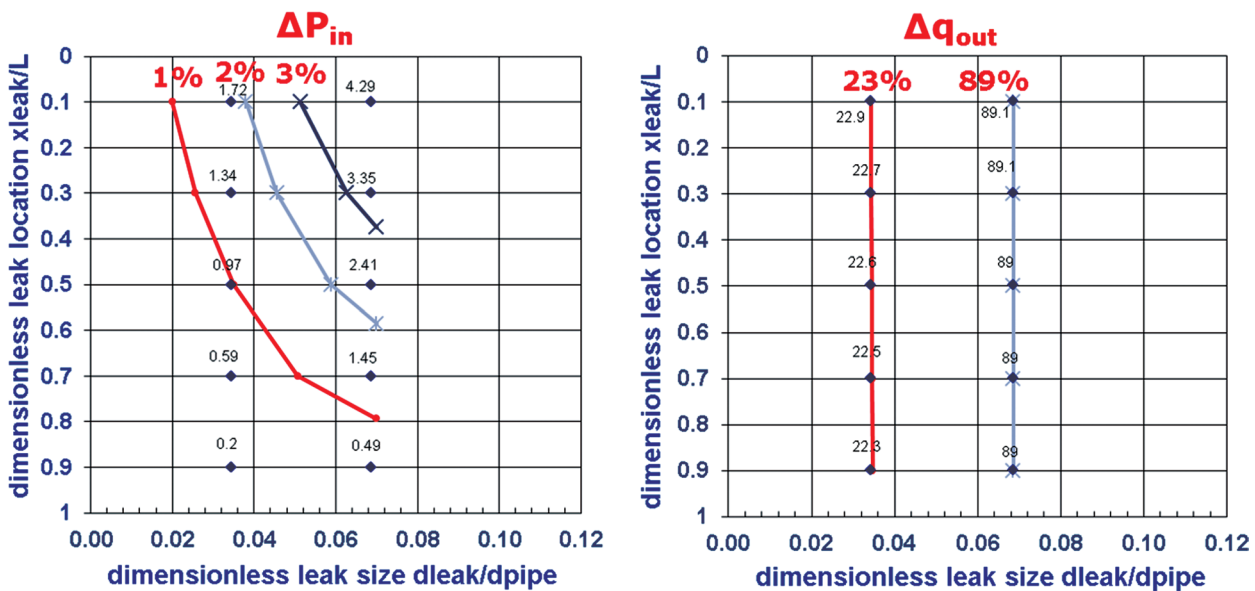
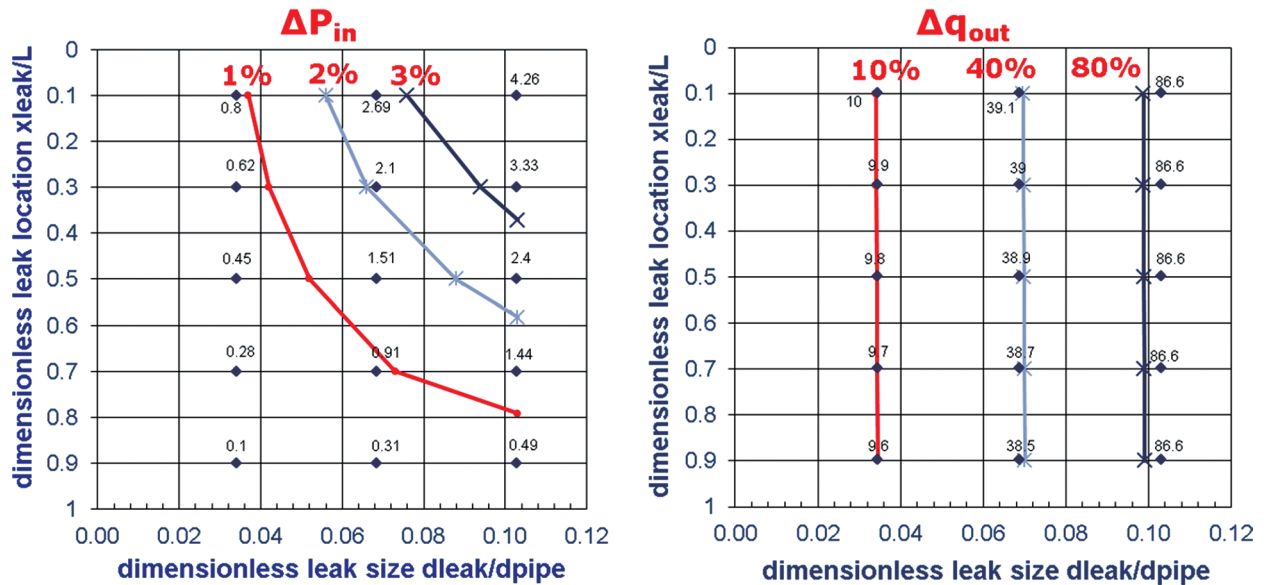


Figure 10 Contour Plots Showing the Changes in Leak Detection Indicators with and without Leak for the Largest  $C_D$  ( $C_D=4.11$ ): (a) Change in Inlet Pressure ( $\Delta P_{in}$ ), (b) Change in Outlet Flowrate ( $\Delta q_{out}$ )



**Figure 11**  
**Contour Plots Showing the Changes in Leak Detection Indicators with and without Leak for the Second-Largest  $C_D$  ( $C_D=1.78$ ): (a) Change in Inlet Pressure ( $\Delta P_{in}$ ), (b) Change in Outlet Flowrate ( $\Delta q_{out}$ )**

Figures 10 and 11 show the similar contour plots for  $\Delta P_{in}$  and  $\Delta q_{out}$  for Case 2 and Case 3 where  $C_D = 4.11$  and 1.78, respectively. Note that these two  $C_D$  values are the largest and the second-largest from the fit to large-scale experiments in Table 1. The results for  $C_D = 4.11$  do not include the case of  $d_{leak}/d_{pipe} = 0.1030$  because the model predicts the loss of gas mass through the leak should be more than the gas mass flowing within the pipeline, which physically cannot be achieved.

Comparison of these contour plots at three fixed values of  $C_D$  can be made by using Figures 9, 10, and 11 with  $C_D = 0.55, 4.11,$  and  $1.78$  respectively. For example, for a leak with  $x_{leak}/L = 0.5$  and  $d_{leak}/d_{pipe} = 0.0687$ ,  $\Delta P_{in}$  changes from 0.547 to 1.51 and 2.41 %, and  $\Delta q_{out}$  changes from 12.2 to 38.9 and 89.0 %, as  $C_D$  increases from 0.55 to 1.78 and 4.11, respectively (This corresponds to a ratio of 1:2.76:4.41 for  $\Delta P_{in}$  and 1:3.19:7.30 for  $\Delta q_{out}$ , meaning that  $\Delta q_{out}$  increases more than  $\Delta P_{in}$  as  $C_D$  increases).

The following general observations can be made from the comparison: (i) in all three cases, the change in inlet pressure ( $\Delta P_{in}$ ) is smaller than the change in outlet flowrate ( $\Delta q_{out}$ ). This means that the use of  $\Delta q_{out}$  as a leak detection indicator is much more superior to the use of  $\Delta P_{in}$ ; (ii) a larger value of  $C_D$  tends to result in a higher level of disturbance to  $\Delta P_{in}$  and  $\Delta q_{out}$ . This is because more gas can escape through the leak easily with larger  $C_D$  (cf. Equation 10); (iii) for both leak detection indicators of  $\Delta P_{in}$  and  $\Delta q_{out}$ , a leak positioned closer to the inlet with a larger opening size exhibits a higher level of disturbance, implying that a leak with such characteristics can be more easily identified by a modeling approach presented by this study; and (iv) following (iii), when compared to the  $\Delta P_{in}$  contours, the  $\Delta q_{out}$  contours are much steeper showing that the magnitude of  $\Delta q_{out}$  is primarily dependent upon

$d_{leak}/d_{pipe}$  but relatively insensitive to  $x_{leak}/L$ . It should be noticed, however, that this sensitivity is mainly caused by relatively high backpressure ( $P_{out} = 643$  psi) compared to the overall pressure drop ( $\Delta P = P_{in} - P_{out} = 33$  psi). The  $\Delta q_{out}$  contours do become also sensitive to  $x_{leak}/L$  at low backpressure or with long pipeline systems as discussed in the later section.

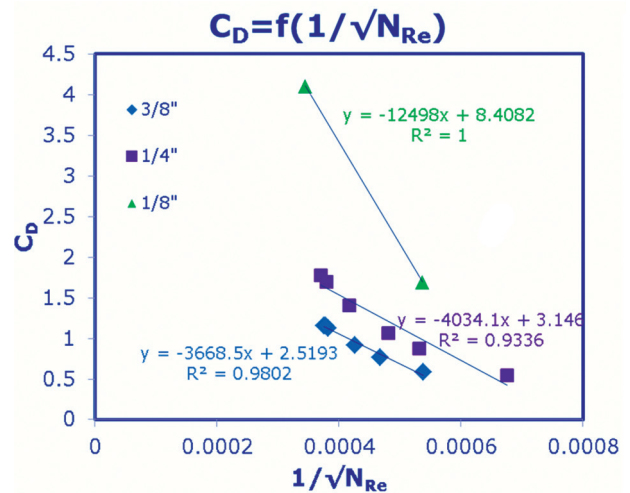


**Figure 12**  
**Relationship Between  $C_D$  and Reynolds Numbers ( $N_{Re}$ ) from the Analysis of Experimental Data and Modeling**

Similar calculations are repeated not by using a fixed value of  $C_D$ , but by making  $C_D$  as a function of Reynolds Number ( $N_{Re}$ ) in Case 4 as described in Equation (11). First, the two parameters in Equation (11), a and b, should be decided from experimental data in Table 1 and Figure 7. We do not know how to interpret the negative  $C_D$  value (i.e.,  $C_D = -0.17$ ) at  $d_{leak} = 1/8$  inches in Table 1, and therefore the Data No. 15 is discarded for the

analysis. Figure 12 shows how  $C_D$  changes as a function of  $N_{Re}^{-1/2}$  for three different leak opening sizes ( $d_{leak} = 1/8, 1/4,$  and  $3/8$  inches) by using the remaining 14 data points. For each  $d_{leak}$ , a best-fit straight line can be determined together with  $R^2$  value, which in turn determines a set of

(a, b). Because these two parameters are affected by leak opening size, a further analysis is performed to extract their relationships as shown in Figures 13 (a) and 13(b). Because it is not certain how a and b should be correlated with  $d_{leak}$ , a simple quadratic curve fitting is used.

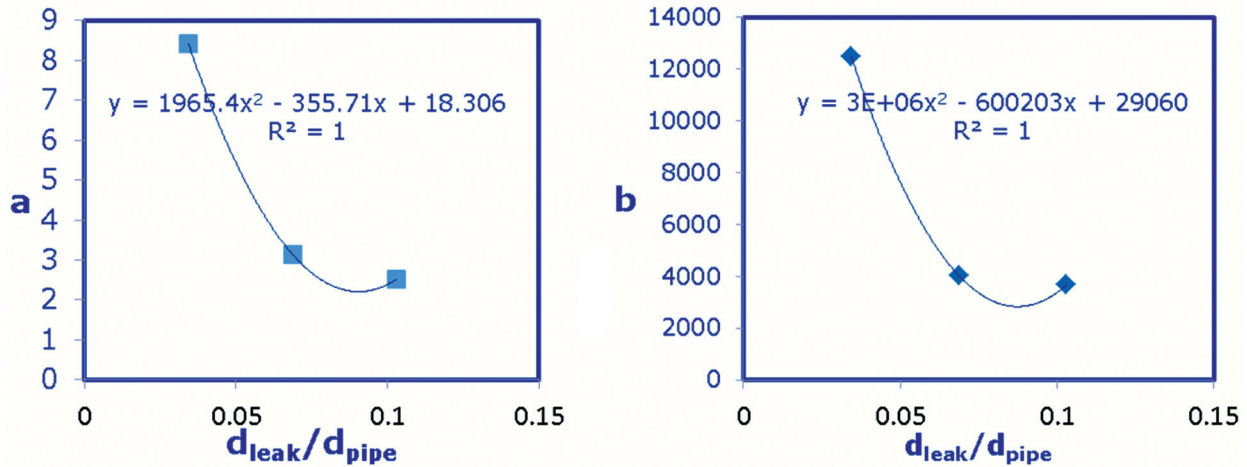


**Figure 13**  
**Determination of Two Model Parameters, “a” and “b”, in Equation (11) to Correlate Leak Coefficient and Reynolds Number**

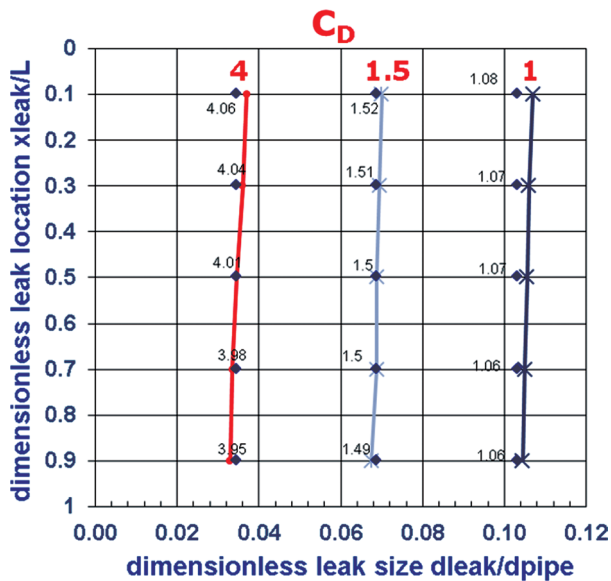


**Figure 14**  
**Contour Plots Showing the Change in Leak Coefficient At Different Leak Locations and Opening Sizes**

Once this analysis is completed by following the steps in Figures 12 and 13, it is possible to reconstruct a map which shows how the leak coefficient ( $C_D$ ) varies as a function of  $x_{leak}/L$  and  $d_{leak}/d_{pipe}$  as shown in Figure 14. Note that the trend in Figure 14 is consistent with the trend in Table 1: higher  $C_D$  values at smaller opening sizes; and higher  $C_D$  values with higher leak rate ( $q_{leak}$ ) represented by leak location closer to the inlet. This allows us to plot similar  $\Delta P_{in}$  and  $\Delta q_{out}$  contours as shown in Figure 15. Note that for calculation of  $C_D$  by using

Equation (11), the effect of  $x_{leak}/L$  is implicitly included in Reynolds number (cf. Equation (12)) through gas phase properties (i.e., density, flow rate, and viscosity), while the effect of  $d_{leak}/d_{pipe}$  is reflected in both (a, b) values (cf. Figures 13(a) and 13(b)) and Reynolds Number. Figure 15 shows that the changes in the two leak detection indicators,  $\Delta P_{in}$  and  $\Delta q_{out}$ , are generally within the two extreme cases of  $C_D$  values (i.e., Figure 9 for  $C_D = 0.55$  and Figure 10 for  $C_D = 4.11$ ). Comparing the magnitudes of  $\Delta P_{in}$  and  $\Delta q_{out}$  in Figures 9, 10, and 15, the use of a fixed value of  $C_D$  may result in a significant error if  $C_D$  is indeed a function of Reynolds Number. It is not clear, however, how to extrapolate this finding to different experimental conditions.

**2.3 Effect of Gas Compressibility on Leak Detection Indicators**

The large-scale experiments of Scott and Yi (1998) has a relatively high outlet pressure compared to the pressure drop between the inlet and outlet, more specifically,  $\Delta P/P_{out} = 32.63/643.37 = 0.0507$  when there is no leak. This implies that even though the gas phase is compressible, the effect of gas compressibility is not pronounced in this particular case due to high back pressure. In order to investigate how the leak detection indicators change for the case when the effect of compressibility is more significant, we examine one more case with the same gas mass rate ( $q_{in} = 5$  MMscf/day) but with much lower  $P_{out}$  of 14.7 psia. Our model shows that the corresponding inlet pressure ( $P_{in}$ ) in this case is about 209.63 psia, which leads to  $\Delta P/P_{out} = (209.63-14.7)/14.7 = 13.26$  in the absence

of leak. It is worth noting that in general a large  $\Delta P/P_{out}$  (meaning a higher level of compressibility effect) may represent either the case with a lower backpressure at the

same inlet gas mass rate and pipeline length, or the case with a longer pipeline length at the same inlet pressure and gas mass rate.

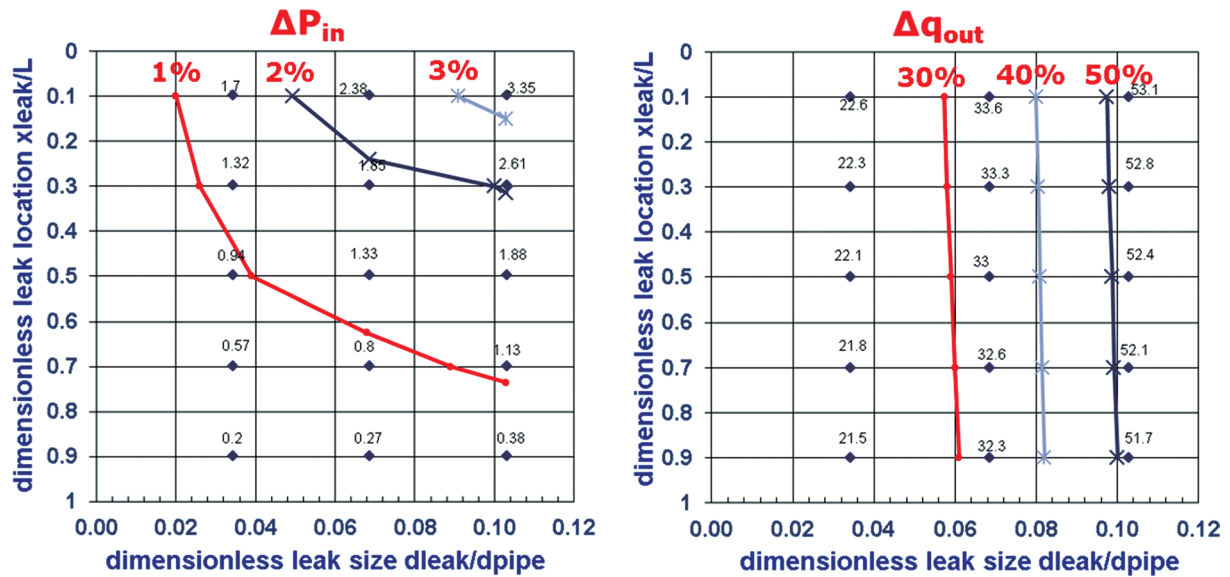


Figure 15  
 Contour Plots Showing the Changes in Leak Detection Indicators with and without Leak for  $C_D$  as a Function of  $N_{Re}$ : (a) Change in Inlet Pressure ( $\Delta P_{in}$ ); (b) Change in Outlet Flowrate ( $\Delta q_{out}$ )

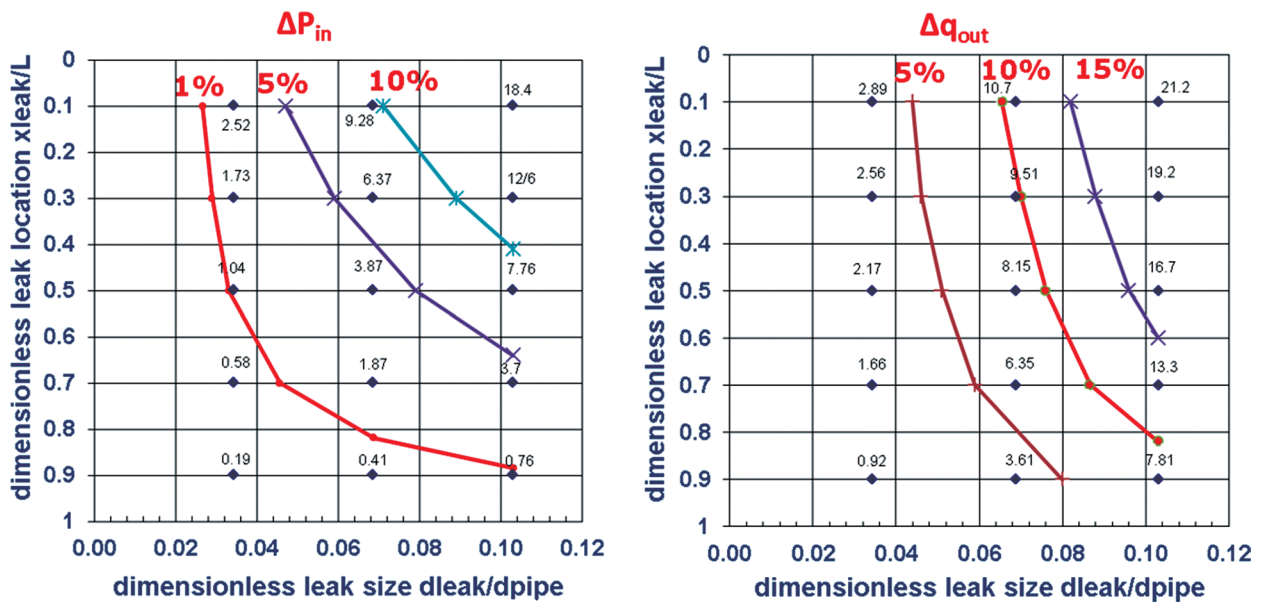


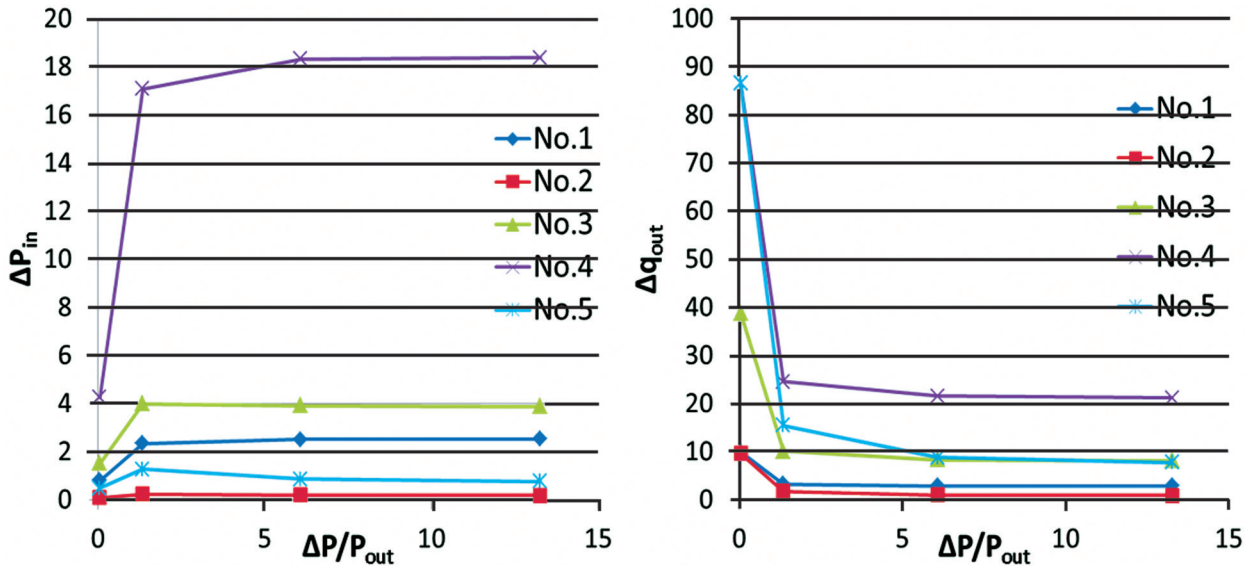
Figure 16  
 Contour Plots Showing the Changes in Leak Detection Indicators for  $C_D = 1.78$  and  $P_{out} = 14.7$  psia to be Compared with Figure 11 ( $C_D = 1.78$  and  $P_{out} = 643.37$  psia)

Figure 16 shows the contour plots for  $\Delta P_{in}$  and  $\Delta q_{out}$  when  $C_D = 1.78$  and  $P_{out} = 14.7$  psia, which can be compared and contrasted with Figure 11 ( $C_D = 1.78$  and  $P_{out} = 643.37$  psia). A few important observations can be spotted when the contours with high  $\Delta P/P_{out}$  (Figure 16) are compared with those with low  $\Delta P/P_{out}$  (Figure 11): (i) although the magnitude of  $\Delta P_{in}$  is increased, the magnitude of  $\Delta q_{out}$  is reduced at higher  $\Delta P/P_{out}$ , and; (ii) the  $\Delta q_{out}$  contours at higher  $\Delta P/P_{out}$  are not very steep

- rather the slopes are now comparable with the  $\Delta P_{in}$  contours. This is because the leak near the inlet has more compressed gas relatively. The former is contradictory to the results in Kam (2010) which observed an increase in both  $\Delta P_{in}$  and  $\Delta q_{out}$  with a reduction in backpressure from two-phase gas-liquid leak detection modeling. A further investigation shows that this difference is caused by the fact that a leak in single gas-phase pipelines, as shown in this study, always reaches a sonic flow in which the

calculation of  $q_{leak}$  requires only downstream pressure ( $P_{sur}$  in Equation(10)); while a leak in pipelines with a relatively large quantity of liquid, as shown in Kam (2008),

is always a sub-sonic flow in which the calculation of  $q_{leak}$  requires both upstream pressure (i.e.,  $P_{leak}$ ) and downstream pressure ( $P_{sur}$ ).



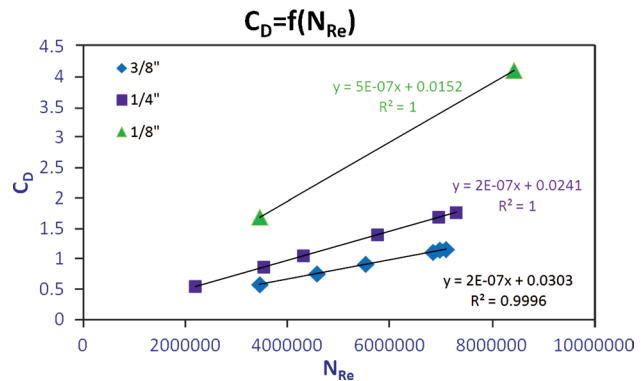
**Figure 17**  
**Changes in Leak Detection Indicator ( $P_{in}$  and  $q_{out}$ ) in a Wide Range of  $DP/P_{out}$  at Different Leak Sizes and Locations: No 1,  $x_{leak}/L = 0.1$  and  $d_{leak}/d_{pipe} = 0.0343$ ; No 2,  $x_{leak}/L = 0.1$  and  $d_{leak}/d_{pipe} = 0.1030$ ; No 3,  $x_{leak}/L = 0.5$  and  $d_{leak}/d_{pipe} = 0.0687$ ; No 4,  $x_{leak}/L = 0.9$  and  $d_{leak}/d_{pipe} = 0.0343$ ; and No 5,  $x_{leak}/L = 0.9$  and  $d_{leak}/d_{pipe} = 0.1030$**

Figure 17 shows the changes in  $\Delta P_{in}$  and  $\Delta q_{out}$  in a wide range of  $\Delta P/P_{out}$ , by repeating the same calculations described in Figure 16 with  $q_{in} = 5$  MMscf/day and  $C_D = 1.78$ . For comparison, we select five different leak characteristics: No. 1,  $x_{leak}/L = 0.1$  and  $d_{leak}/d_{pipe} = 0.0343$ ; No. 2,  $x_{leak}/L = 0.1$  and  $d_{leak}/d_{pipe} = 0.1030$ ; No. 3,  $x_{leak}/L = 0.5$  and  $d_{leak}/d_{pipe} = 0.0687$ ; No. 4,  $x_{leak}/L = 0.9$  and  $d_{leak}/d_{pipe} = 0.0343$ ; and No. 5,  $x_{leak}/L = 0.9$  and  $d_{leak}/d_{pipe} = 0.1030$ . The results indicate that both  $\Delta P_{in}$  and  $\Delta q_{out}$  are very sensitive to  $\Delta P/P_{out}$ , and which one of those two leak detection indicators is more reliable strongly depends on the level of  $\Delta P/P_{out}$ .

### 2.4 Reynolds Number ( $N_{Re}$ ) Dependent Leak Coefficient ( $C_D$ )

As pointed out earlier, the previous experimental studies show that the leak coefficient ( $C_D$ ) is proportional to  $N_{Re}^{-1/2}$  as shown in Equation (11), and therefore we correlated the experimental data to that equation in order to extract model parameters, a and b, in Figure 13. We do not know, however, if this particular relationship between  $C_D$  and  $N_{Re}$  from small-scale experiments using nozzles and chokes is still applicable to pipeline leak detection modeling. For example, Figure 18 shows a plot of  $C_D$  as a function of  $N_{Re}$  rather than  $N_{Re}^{-1/2}$ . Compared with Figure 12, this plot shows a better fit to experimental data in Table 1 with improved  $R^2$  values. This implies that the typical level of  $C_D$  values can be decided by the method presented in this study (cf. Table 1), but it is still not clear how to express  $C_D$  as a function of other experimental conditions. This

indirectly tells us how complicated pipeline leak detection is, and suggests where the foci of future studies should be made.



**Figure 18**  
**The Relationship Between  $C_D$  and Reynolds Numbers ( $N_{Re}$ ) if  $C_D$  is Proportional to  $N_{Re}$ , Rather than  $N_{Re}^{-1/2}$ , from the Analysis of Experimental Data and Modeling**

## CONCLUSION

This pipeline leak detection modeling study for a single-phase gas flow can be summarized as follows:

- (i) A leak detection model for a single gas-phase flow is constructed in order to quantify the level of disturbance in the system by comparing a steady state with no leak and the other steady state with leak. The model uses two leak detection indicators - the change in inlet pressure ( $\Delta P_{in}$ ) and the change in outlet flow rate ( $\Delta q_{out}$ ) - by fixing inlet flow rate ( $q_{out}$ ) and outlet pressure ( $P_{out}$ ). The key

concepts associated with this modeling technique are material balance and pressure traverse calculations.

(ii) Previous modeling studies show that the leak coefficient ( $C_D$ ), a parameter that defines how easily gas phase can escape through the leak, is a single-most important parameter whose magnitude is largely unknown. When this new model is matched with large-scale experimental data from Scott and Yi (1998), which are from 9,460-ft length 3.64-inch inner diameter horizontal flow loops with leak opening-size diameter of 1/8 to 3/8 inches located in the middle of the pipeline, the results show that the range of  $C_D$  values is around 0.55 to 4.11 with a relatively larger magnitude for a leak with a smaller opening size positioned near the inlet. Although the model fit proves the dependence of  $C_D$  values on Reynolds Number ( $N_{Re}$ ), it is not clear exactly what functions should be used to relate them. The correlations developed from previous small-scale experiments show  $C_D \sim N_{Re}^{-1/2}$  but the analysis in this study shows  $C_D \sim N_{Re}$ .

(iii) When the two leak detection indicators ( $\Delta P_{in}$  and  $\Delta q_{out}$ ) are plotted in a form of contours, leaks present near the inlet with bigger opening sizes exhibit larger  $\Delta P_{in}$  and  $\Delta q_{out}$ , implying such leaks can be more easily identified by a modeling technique introduced in this study. As the effect of gas compressibility increases (i.e., the pressure drop between the inlet and the outlet of pipeline is relatively larger compared to the outlet pressure), the magnitude of  $\Delta P_{in}$  increases while the magnitude of  $\Delta q_{out}$  decreases. For practical applications, this implies that the two indicators should be used together to check the presence of leak if possible. Taking the magnitude into consideration,  $\Delta q_{out}$  is a better indicator than  $\Delta P_{in}$  when gas compressibility is negligible, and  $\Delta P_{in}$  is a better indicator than  $\Delta q_{out}$  when gas compressibility is significant.

## ACKNOWLEDGEMENT

We would like to express our special thanks to Chevron, Inc. for financial support. Additional support was provided by Donald W. and Gayle A. Keller Distinguished Professorship.

## REFERENCES

- [1] Arnold, K., & Stewart, M. (1999). *Surface Production Operations* (Volume 2). Houston, Tx: Gulf Publishing Company.
- [2] Ashford, F. E., & Pierce, P. E. (1975). Determining Multiphase Pressure Drops and Flow Capacities in Down-Hole Safety Valves. *Journal of Petroleum Technology*, 27(9), 1145-1152.
- [3] Berton, J. (2010). San Bruno's 8<sup>th</sup> Fatality from PG&E Blast. *San Francisco Chronicle*. Retrieved from <http://www.sfgate.com/cgi-bin/article.cgi?f=/c/a/2010/09/28/BAIQ1FKVE5.DTL&type=health>
- [4] Chen, N. H. (1979). An Explicit Equation for Friction Factor in Pipe. *Ind. Eng. Chem. Fundam.*, 18(3), 296-297.
- [5] Crane Company. (1957). *Flow of Fluids Through Valves, Fittings, and Pipe* (TP 410). New York, N.Y.
- [6] Danesh, A. (1998). *PVT and phase behaviour of petroleum reservoir fluids*. Amsterdam: Elsevier.
- [7] Dranchuk, P. M., & Abou-Kassem, J. H. (1975). Calculation of z-Factors for Natural Gases Using Equations of State. *Journal of Canadian Petroleum Technology*, 14(3), 34-36.
- [8] Gajbhiye, R. N., & Kam, S. I. (2008). Leak Detection in Subsea Pipeline: a Mechanistic Modeling Approach with Fixed Pressure Boundaries. *SPE Projects, Facilities, and Construction*, 3(4), 1-10.
- [9] Guo, B., Lyons, W. C., & Ghalambor, A. (2007). *Petroleum Production Engineering, a Computer-Assisted Approach*. Gulf Professional Publishing.
- [10] Guo, B., Al-Bemani, A. S., & Ghalambor, A. (2002). *Applicability of Sachdeva's Choke Flow Model in Southwest Louisiana Gas Condensate Wells*. Paper Presented at the *SPE Gas Technology Symposium*, Calgary, Alberta.
- [11] Gilbert, W. E. (1954). Flowing and Gas-Lift Well Performance. *Drill. & Prod. Practice*, 126.
- [12] Hoeffel, J., Hennessy-Fiske, M., & Goffard, C. (2010). San Bruno Explosion Death Toll Climbs to Seven; Six are Missing. *Los Angeles Times*. Retrieved from <http://www.latimes.com/news/local/la-me-0912-san-bruno-explosion-20100912,0,251794.story>
- [13] Ishibashi, M., & Takamoto, M. (2000). Theoretical Discharge Coefficient of a Critical Circular-Arc Nozzle with Laminar Boundary Layer and Its Verification by Measurements Using Super-Accurate Nozzles. *Flow Measurement and Instrumentation*, 11(4), 305-313.
- [14] Kam, S. I. (2010). Mechanistic Modeling of Pipeline Leak Detection at Fixed Inlet Rate. *Journal of Petroleum Science and Engineering*, 70(3), 145-156.
- [15] Kim, J. H., Kim, H. D., & Park, K. A. (2006). Computational/ Experimental Study of a Variable Critical Nozzle Flow. *Flow Measurement and Instrumentation*, 17, 81-86.
- [16] Lee, A., Gonzalez, M. H., & Eakin, B. E. (1966). The Viscosity of Natural Gases. *Journal of Petroleum Technology*, 18(8), 997-1000.
- [17] Minerals Management Services. (2009). *Gulf of Mexico oil and gas production forecast: 2009-2018* (OCS Report MMS 2009-012). Retrieved from <http://www.gomr.boemre.gov/>
- [18] Moody, L. F. (1944). Friction Factors for Pipe Flow. *Transactions of the ASME*, 66(8), 671-684.
- [19] Morris, S. D. (1996). Choke Pressure in Pipeline Restrictions. *Journal of Hazardous Materials*, 50(1), 65-69.
- [20] Papadakis, G. A., Porter, S., & Wettig, J. (1999). EU Initiative on the Control of Major Accident Hazards Arising from Pipelines. *Journal of Loss Prevention in the Process Industries*, 12(1), 85-90.
- [21] Papadakis, G. A. (1999). Major Hazard Pipelines: a Comparative Study of Onshore Transmission Accidents. *Journal of Loss Prevention in the Process Industries*, 12(1), 91-107.

- [22] Payne, M. L. (2007). Deepwater Activity in the US Gulf of Mexico Continues to Drive Innovation and Technology. *Exploration & Production: The Oil and Gas Review 2007 - OTC Edition*.
- [23] Richardson, S. M., Saville, G., Fisher, A., Meredith, A. J., & Dix, M. J. (2006). Experimental Determination of Two-Phase Flow Rates of Hydrocarbons Through Restrictions. *Process Safety and Environmental Protection*, 84(1), 40-53.
- [24] Richardson, G. E., Nixon, L. D., Bohannon, C. M., Kazanis, E. G., Montgomery, T. M., & Gravois, M. P. (2008). *Deepwater Gulf of Mexico 2008: America's Offshore Energy Future*. U.S. Dept. of the Interior, Minerals Management Service, Gulf of Mexico OCS Region, New Orleans, LA.
- [25] Ros, N. C. J. (1960). An Analysis of Critical Simultaneous Gas/Liquid Flow Through a Restriction and Its Application to Flowmetering. *Applied Scientific Research*, 9(1), 374-388.
- [26] Rosen, Y., & Schneyer, J. (2011). Alaska Pipeline Restart Unknown; Oil up, BP Dips. *Reuters*. Retrieved from <http://www.reuters.com/article/2011/01/10/us-oil-pipeline-alaska-idUSTRE7080H820110110>
- [27] Sachdeva, R., Schmidt, Z., Brill, J. P., & Blais, R. M. (1986, October). *Two-Phase Flow Through Chokes*. Paper Presented at the SPE Annual Technical Conference and Exhibition, New Orleans, Louisiana.
- [28] Scott, S. L., & Barrufet, M. A. (2003). *Worldwide Assessment of Industry Leak Detection Capabilities for Single & Multiphase Pipelines* (PB2011-104131). Minerals Management Service.
- [29] Scott, S. L., & Yi, J. (1998). *Detection of Critical Flow Leaks in Deepwater Gas Flowlines*. Paper Presented at the SPE Annual Technical Conference and Exhibition, New Orleans, LA.
- [30] Simonoff, J. S., Restrepo, C. E., & Zimmerman, R. (2010). Risk Management of Cost Consequences in Natural Gas Transmission and Distribution Infrastructures. *Journal of Loss Prevention in the Process Industries*, 23(2), 269-279.
- [31] U.S. Department of Transportation's Pipeline and Hazardous Materials Safety Administration. (2010). *PHMSA significant incident files*. Retrieved from [www.phmsa.dot.gov](http://www.phmsa.dot.gov)
- [32] Wang, S., & Carroll, J. J. (2007). Leak Detection for Gas and Liquid Pipelines by Transient Modeling. *SPE Projects, Facilities & Construction*, 2(2), 1-9.